Supporting Information

Comparison of UV Irradiation and Sintering on Mesoporous Spongelike ZnO Films Prepared from PS-b-P4VP Templated Sol-Gel Synthesis

Kun Wang[a], *Senlin Xia*[a], *Wei Cao* [a], *Nuri Hohn* [a], *Sebastian Grott* [a], *Lucas P. Kreuzer* [a], *Matthias Schwartzkopf*[b], *Stephan V. Roth* [b,c], *Peter Müller-Buschbaum* [a,d]*

[a]Lehrstuhl für Funktionelle Materialien, Physik-Department, Technische Universität München, James-Franck-Strasse 1, 85748 Garching, Germany

[b]Deutsches Elektronen-Synchrontron (DESY), Notkestrasse 85, 22603 Hamburg, Germany

[c]KTH Royal Institute of Technology, Department of Fibre and Polymer Technology, Teknikringen 56-58, SE-100 44 Stockholm, Sweden

[d]Heinz Maier-Leibnitz Zentrum (MLZ), Technische Universität München, Lichtenbergstr. 1, 85748 Garching, Germany

Corresponding Author

* E-Mail: muellerb@ph.tum.de; Phone: +49 89 289 12451; Fax: +49 89 289 12 473

FT-IR spectra

FT-IR spectra of the films are shown in Figure S1 before and after applying the post-treatment method (namely sintering or UV-irradiation) to remove the polymer template. For the films without post-treatment, the curve shows strong absorption peaks at 1621 and 700 cm^{-1}, which are attributed to the stretching modes of pyridine rings and aromatic rings, respectively, indicating the existence of P4VP and PS blocks.[1] In contrast, these peaks disappear for the samples after post-treatment with either sintering or UV-irradiation, suggesting that the polymer template is removed completely by either sintering or UV-irradiation.

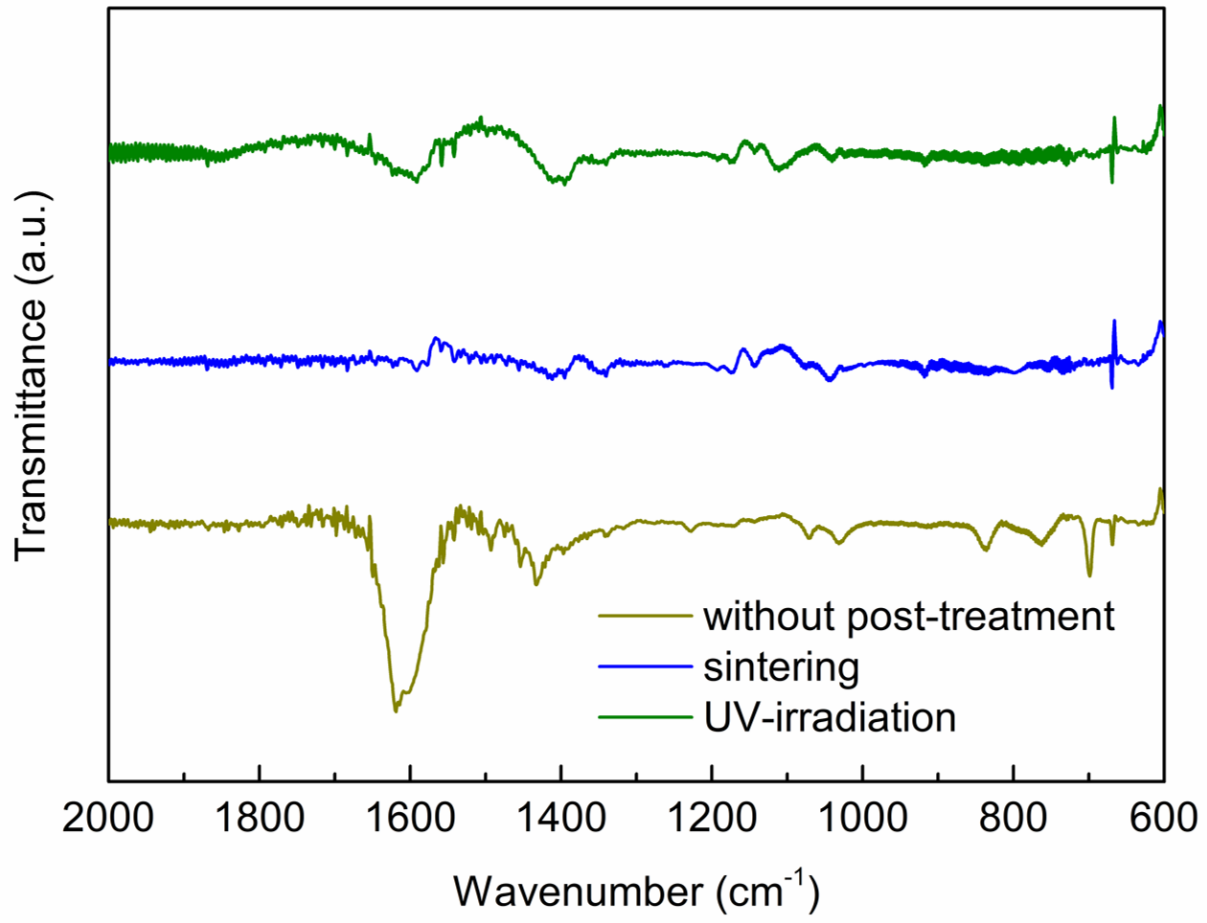

Figure S1. FTIR spectra of ZnO/PS-b-P4VP composite films (prepared from the polymer template-to-ZAD ratio of 5:12) without post-treatment and the corresponding ZnO films after polymer extraction via sintering or UV-irradiation.

XRD data

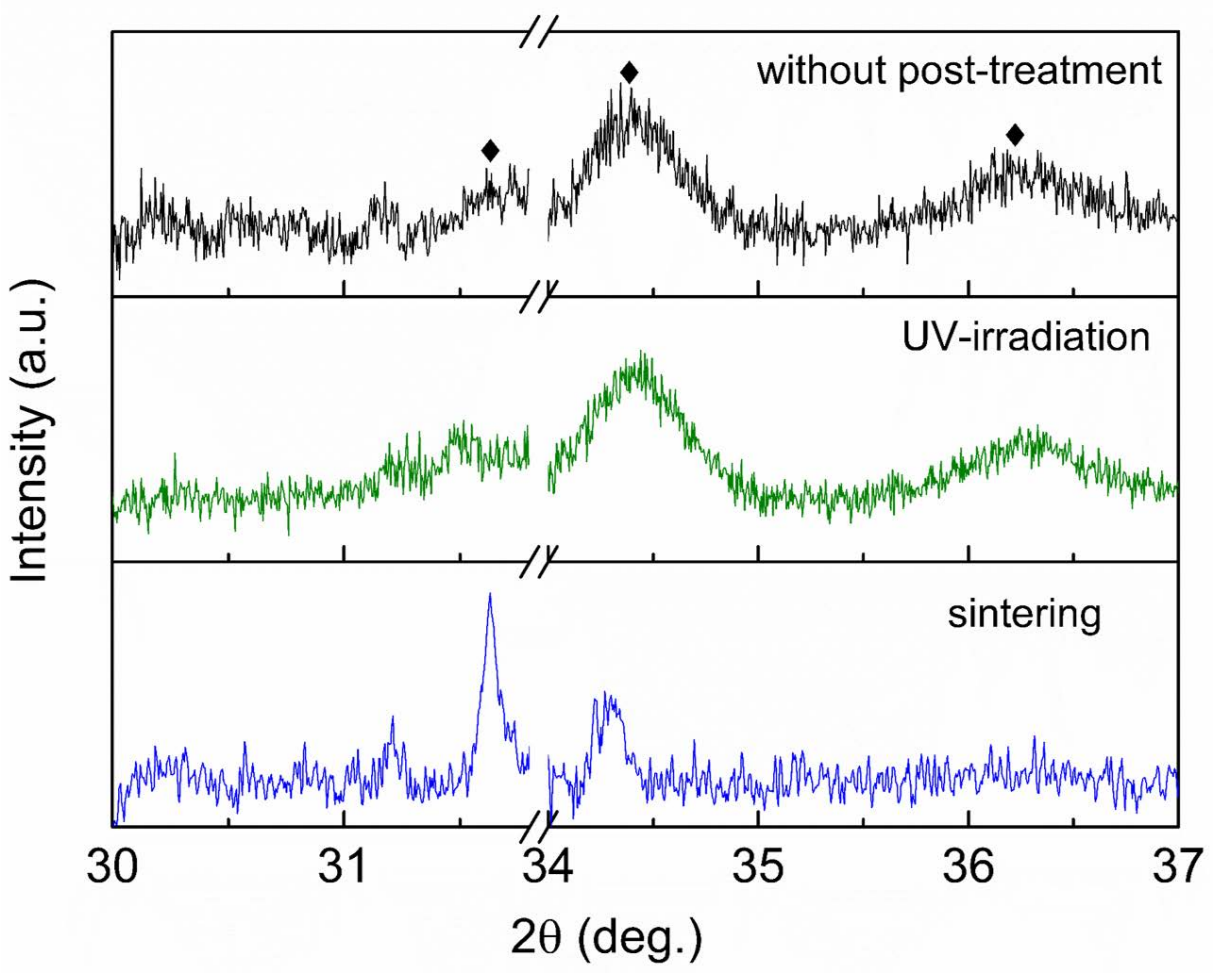

Figure S2. XRD patterns of ZnO/PS-b-P4VP (without post-treatment) and mesoporous ZnO films after polymer removal by UV-irradiation and sintering. The Bragg peaks at around 31.6, 34.3, and 36.3 deg. correspond to crystal planes of (100), (002) and (101), respectively. The curves are interrupted from 31.8 to 34 deg. to remove the strong Bragg peak of the Si substrate. The Bragg peaks of ZnO wurtzite phase are indicated by diamonds.

SEM data

To further investigate the influence of ratio (polymer template to ZAD) on the morphology tuning, ZnO films annealed at 240 °C (template removed by UV-irradiation) are investigated by SEM (Figure S3) and AFM measurements (Figure S4). At 240 °C, the morphologies of the ZnO films prepared from four different weight ratios are completely different from those annealed at 160 °C. Instead of polymer self-assembly, the incompatibility between PS and P4VP blocks decreases dramatically at 240 °C, which results in ZnO clusters aggregating into larger ones.[2] Moreover, with increasing the ratio of the template, both ZnO clusters and pores become larger which is consistent with the morphology evolution trend at 160 °C.

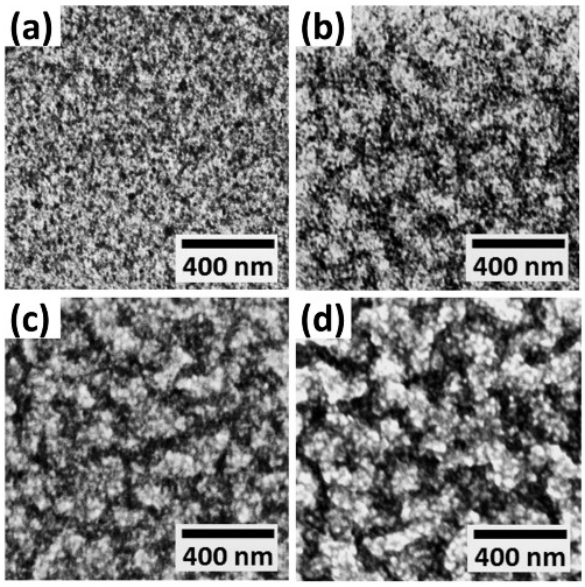

Figure S3. SEM images of UV-irradiated mesoporous ZnO films prepared from different ratios of polymer to ZAD at the annealing temperature of 240 °C: (a) $\omega_{PS\text{-}b\text{-}P4VP}$:$\omega_{ZAD}$=1:12, (b) 3:12, (c) 5:12, and (d) 7:12.

AFM data

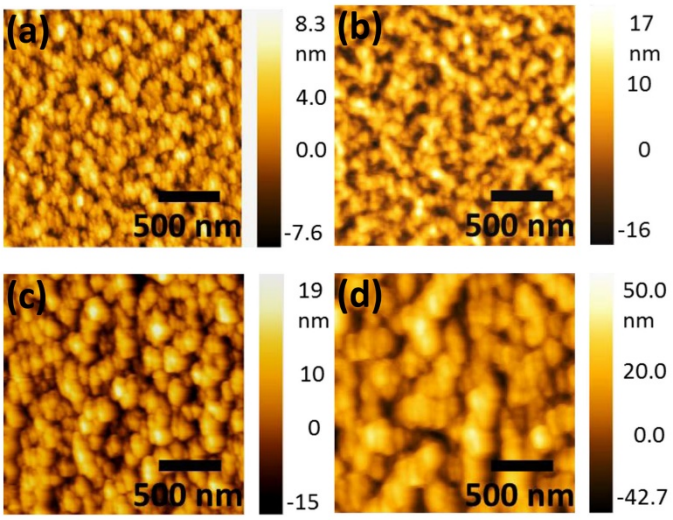

Figure S4. AFM images of UV-irradiated mesoporous ZnO films prepared from different ratios of polymer to ZAD at the annealing temperature of 240 °C: (a) $\omega_{PS\text{-}b\text{-}P4VP}$:$\omega_{ZAD}$=1:12, (b) 3:12, (c) 5:12, and (d) 7:12.

GISAXS data modeling

In order to extract the information of the pores buried in the films, the GISAXS data are modeled in the framework of the effective interface approximation of the distorted wave Born approximation (DWBA). In this approximation, the diffuse scattering factor $P_{diff}(\vec{q})$ (proportional to the recorded intensity) is assumed to be

$P_{diff}(\vec{q}) \propto N|F(\vec{q})|^2 S(\vec{q})$,

in which N is the number of the scattering objects. $F(\vec{q})$ is the form factor which describes the shape and size of the scattering objects. $S(\vec{q})$ is the structure factor, which describes the spatial distribution of the objects. In this model, the local monodisperse approximation (LMA) is used to account for objects with different sizes. It is assumed that each object in the film only scatters with those of similar form and structure factors, rather than with those of different form and structure factors. Therefore, the total scattered intensity can be approximated by incoherently superposing the scattering intensities of the individual objects that appear within the film, if the length scales of the distinct objects are sufficiently different.[3] In the present work, standing cylinders with Gaussian distributed radii are used to describe the form factor due to the thin film geometry and inspired by the SEM pictures. A Gaussian distributed center-to-center distance is assigned to describe the structure factor as shown in Figure S5. We assumed a 1D paracrystalline arrangement of the object as proposed by Hosemann et al.[4] Three such distinct objects (small-, middle- and large-sized structures) are approximated by standing cylinders with Gaussian distribution for the form and structure factors. The resulting fits (solid red lines) are plotted together with the horizontal line cuts in Figure 5a and 5c. The fits are in excellent agreement with the experimental data.

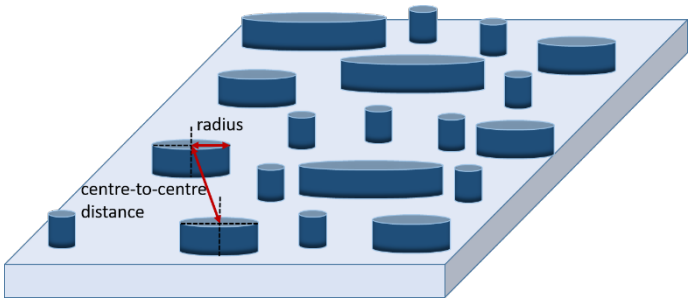

Figure S5. Sketch of the scattering objects used for modelling of the film morphology in the GISAXS data analysis.

In the case of ZnO films, the diameters of these cylindrical objects obtained from the fits denote the size of the ZnO domains. The structure factors obtained from the fits, on the other hand, account for the center-to-center distance between the scattering objects. Values of the average pore size of the ZnO films can then be extracted from the form and the structure factors via

Pore size = (center-to-center distance between the domains - 2 x radius of the domains).

Optical performance

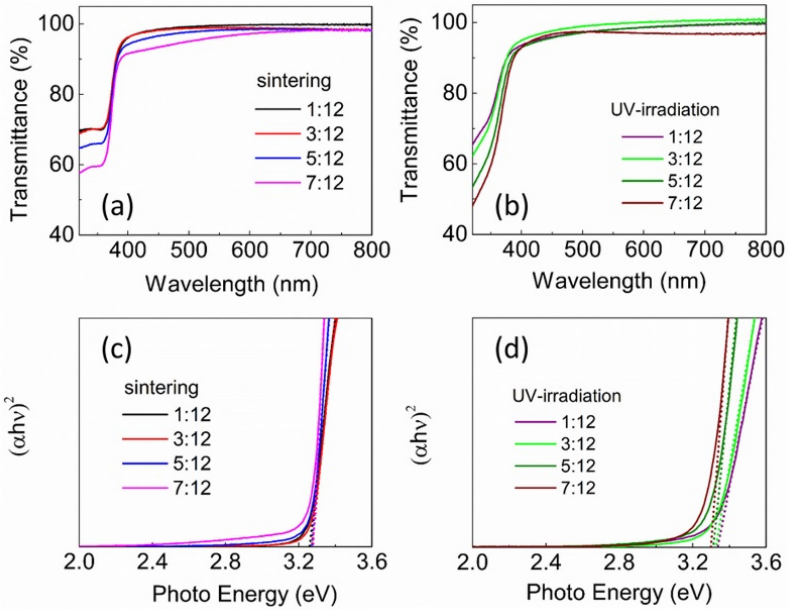

Figure S6. Transmittance spectra and Tauc plots of mesoporous ZnO films prepared from different ratios of polymer to ZAD as indicated at the annealing temperature of 160 °C: (a) and (c) post-treated by sintering, and (b) and (d) post-treated by UV-irradiation.

Device analysis

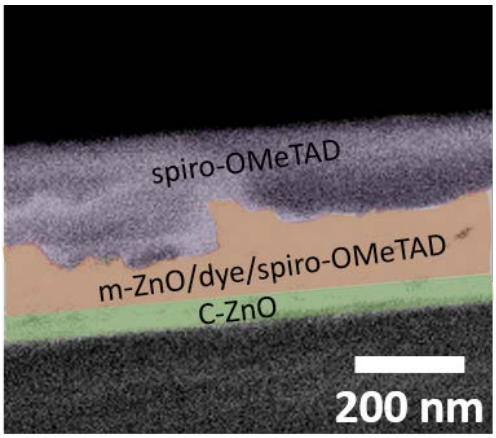

Figure S7. Cross-section SEM view of a ssDSSC based on sintered mesoporous ZnO films with the template-to-ZAD ratio of 5:12. The film thickness of the m-ZnO/dye/spiro-OMeTAD layer is consistent with the ZnO film thickness in Figure 6. FTO is not observed in this section due to etching with zinc powder and hydrochloric acid.

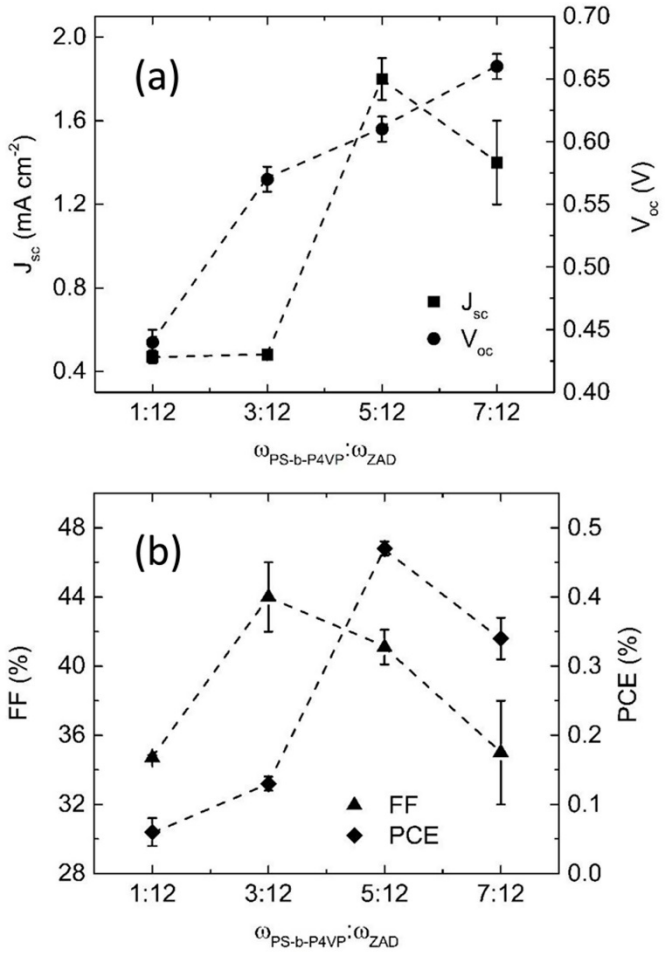

Figure S8. (a) J_{sc} and V_{oc}, (b) FF and PCE extracted from J-V curves of the ssDSSCs based on sintered mesoporous ZnO films plotted as a function of the increasing ratio of polymer to ZAD. The dashed lines are guides to the eye.

Table S1. Device parameters extracted from J-V curves of ssDSSCs based on different post-treated mesoporous ZnO films annealed at 160 °C with $\omega_{PS\text{-}b\text{-}P4VP}$:$\omega_{ZAD}$=5:12.

post-treatment	J_{sc} (mA cm^{-2})	V_{oc} (V)	FF (%)	PCE (%)
UV-irradiation	0.8 ± 0.2	0.68 ± 0.01	39.6 ± 2.0	0.2 ± 0.04
sintering	1.8 ± 0.1	0.61 ± 0.01	41.1 ± 1.0	0.47 ± 0.01

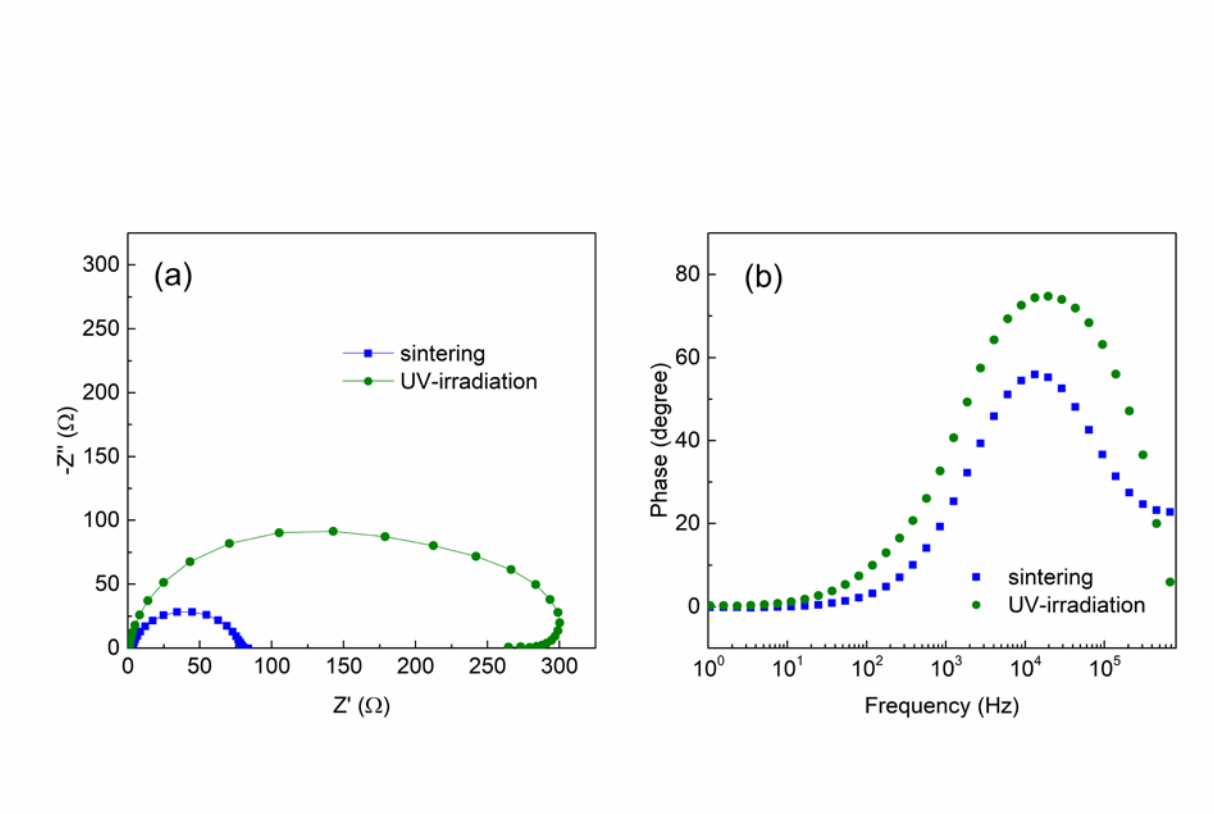

Figure S9. EIS analysis of DSSCs based on ZnO films post-treated with sintering and UV-irradiation as indicated. (a) Nyquist plots; (b) Bode phase plots.

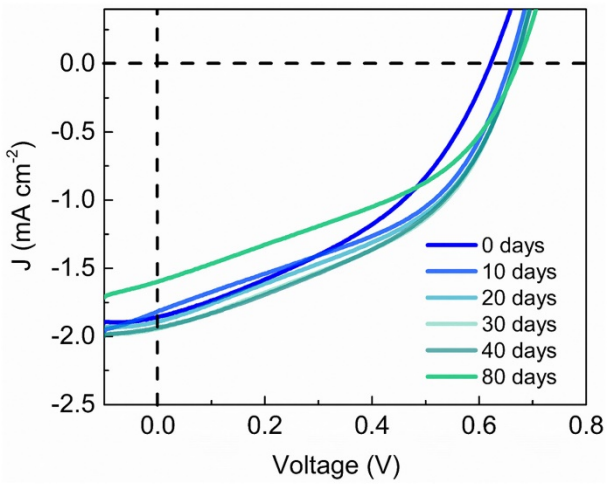

Figure S10. Current-voltage characteristics of ssDSSCs based on sintered nanoporous ZnO films annealed at 160 °C with $\omega_{PS\text{-}b\text{-}P4VP}$:$\omega_{ZAD}$=5:12.

References:

1. Du, B.; Chen, X.; Zhao, B.; Mei, A.; Wang, Q.; Xu, J.; Fan, Z. Interfacial entrapment of noble metal nanoparticles and nanorods capped with amphiphilic multiblock copolymer at a selective liquid–liquid interface. *Nanoscale*, **2010**, *2*, 1684-1689.

2. Swann, J. M. G.; Topham, P. D. Design and application of nanoscale actuators using block-copolymers. *Polymers*, **2010**, *2*, 454-469.

3. Renaud, G.; Lazzari, R.; Leroy, F. Probing surface and interface morphology with grazing incidence small angle X-ray scattering. *Surf. Sci. Rep.*, **2009**, *64*, 255-380.

4. Hosemann, R.; Vogel, W.; Weick, D.; Balta-Calleja, F. Novel aspects of the real paraerystal. *Acta Crystallogr. Sec. A*, **1981**, *37*, 85-91.